LOCKHEED MARTIN ENERGY RESEARCH LIBRARIES
3 4456 0514398 4

CENTRAL RESEARCH LIBRARY
DOCUMENT COLLECTION

OAK RIDGE NATIONAL LABORATORY
operated by
UNION CARBIDE CORPORATION
for the
U. S. ATOMIC ENERGY COMMISSION

ORNL-TM-3262
cy. 55
DATE - December 21, 1970

If you wish someone else to see this document, send in name with document and the library will arrange a loan.
UCN-7969
(3 3-67)

OAK RIDGE NATIONAL LABORATORY
CENTRAL RESEARCH LIBRARY
DOCUMENT COLLECTION
LIBRARY LOAN COPY
DO NOT TRANSFER TO ANOTHER PERSON

Neutron Physics Division

CALCULATION OF THE LONG-LIVED ACTIVITY IN SOIL PRODUCED BY 500-GeV PROTONS*

T. A. Gabriel and R. T. Santoro

Abstract

Calculations have been made to estimate the time and spatial dependence of the long-lived ($\tau_{1/2} \geq 1$ day) activity in the soil surrounding a semi-infinite beam target tunnel. The activity distributions are given for 500-GeV protons incident on a Be target positioned in the tunnel for an irradiation time of 25 years at 10^{13} protons per second and at a time after shutdown of one month. The distributions are presented as a function of the radial distance from the tunnel axis for the spatial regions along the tunnel and at the end of the tunnel. The activity arising from selected nuclides is given for selected spatial points. Curves showing the decrease in activity as a function of shutdown time are given. Included is the calculated integrated activity along the tunnel axis.

*Submitted for journal publication.

NOTICE This document contains information of a preliminary nature and was prepared primarily for internal use at the Oak Ridge National Laboratory. It is subject to revision or correction and therefore does not represent a final report.

This report was prepared as an account of work sponsored by the United States Government. Neither the United States nor the United States Atomic Energy Commission, nor any of their employees, nor any of their contractors, subcontractors, or their employees, makes any warranty, express or implied, or assumes any legal liability or responsibility for the accuracy, completeness or usefulness of any information, apparatus, product or process disclosed, or represents that its use would not infringe privately owned rights.

1. INTRODUCTION

Calculations have been made to determine the long-lived induced activity in the soil surrounding a target tunnel when 500-GeV protons are incident on a thick Be target in the tunnel. In a previous paper[1]), similar calculations were performed, but because of the lack of particle-production data from nucleon- and pion-nucleus collisions and nucleon- and pion-nucleon collisions above 3 GeV, many simplifying assumptions had to be made and the results obtained were considered to be very approximate. Since then, methods for obtaining these particle-production data above 3 GeV have been developed by utilizing two appropriate scaling models[2]) to account for the high-energy collisions. These models are extrapolation procedures which relate the differential cross sections for nucleons and pions from nucleon- and pion-nucleus collisions (Model 1) and nucleon- and pion-nucleon collisions (Model 2) at energies > 3 GeV to the differential cross sections for nucleon and pion production from similar 3-GeV collisions. The incorporation of the scaling models into the calculations has made it possible to eliminate essentially all of the approximations used in the previous work[1]).

The target tunnel geometry and the methods of calculation are described in Sec. 2. The results are presented and discussed in Sec. 3.

2. CALCULATIONAL DETAILS

The target tunnel geometry, along with the materials considered in the calculation, are shown in Fig. 1. Cylindrical coordinates defined by ρ,z were used with the Be target located at $\rho = 0$ and $z = 0$. The tunnel radius is 45.7 cm (1.5 ft) and extends 600 m in the positive z direction and to infinity in the negative z direction. Outside of, and completely surrounding, the tunnel is the soil of density 2.0 g/cm^3 and composition as described in Table I[3]).

LOCKHEED MARTIN ENERGY RESEARCH LIBRARIES

3 4456 0514398 4

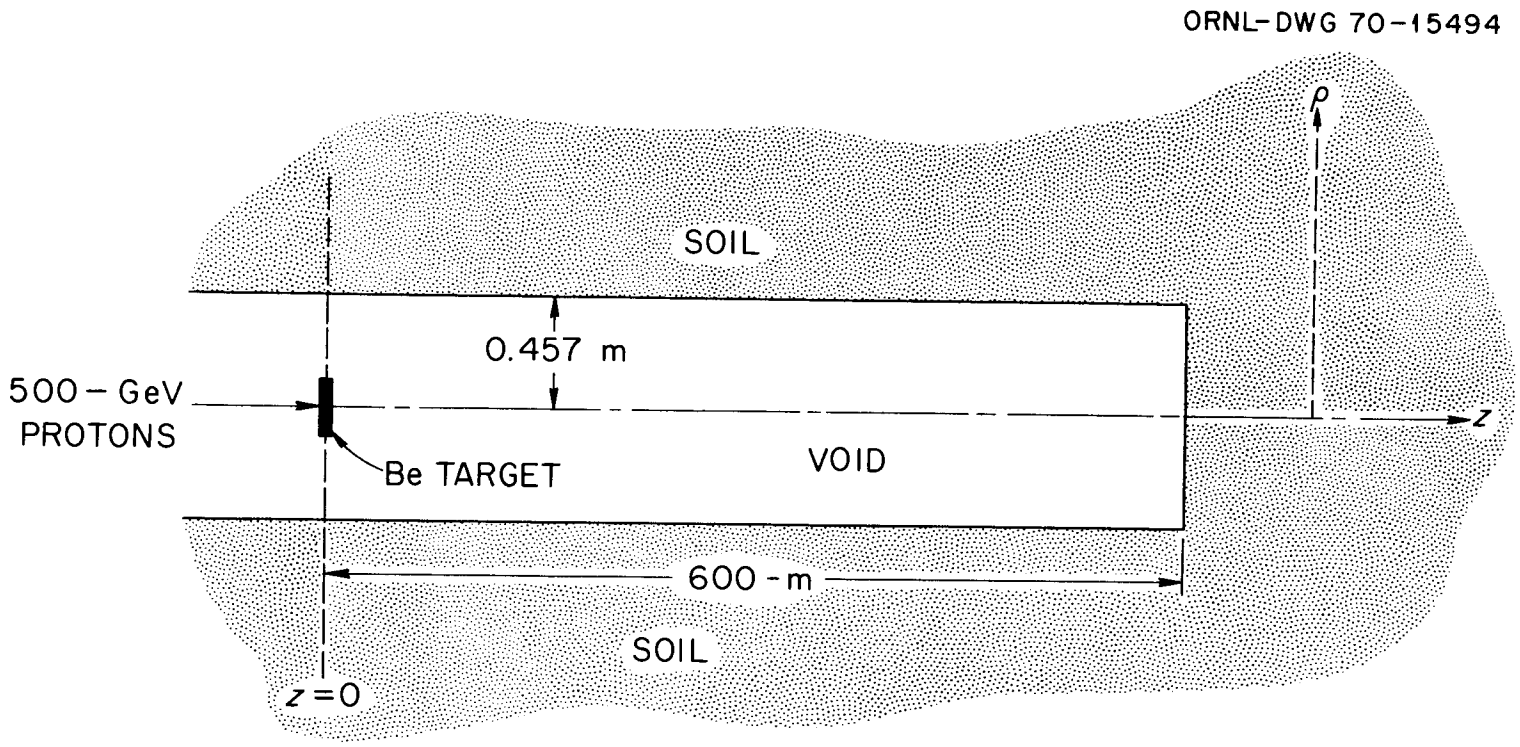

Fig. 1. Schematic Diagram of the Accelerator Target Tunnel.

TABLE I

Composition of Soil

Element	Soil (% by weight)
H	1.23
C	3.32
O	55.03
Na	0.396
Mg	2.09
Al	5.51
Si	22.85
K	0.517
Ca	6.08
Fe	2.91

The calculations presented here were carried out using the high-energy nucleon-meson transport code HETC.* This code, which is similar in structure to NMTC[5]), not only allows for the transport of nucleons and pions below 3 GeV but also gives an accurate representation of the transport of these particles above 3 GeV as well. Monte Carlo methods are employed to transport the primary and secondary particles, and, except for the approximations associated with the collision models, all calculational details are handled rigorously. HETC allows for the continuous slowing down of charged particles, the decay of particles, elastic and nonelastic hydrogen collisions, and nonelastic nuclear interactions. Neutron-nucleus elastic collisions with elements other than hydrogen are neglected above 100 MeV.

In HETC, nonelastic nucleon-nucleus interactions for particles $\leq$ 3 GeV are treated at each appropriate collision site by employing the medium-energy cascade program of Bertini[6]), followed by an evaporation-model calculation[7]) to account for the remaining excitation energy. For energies > 3 GeV, these interactions are accounted for with scaling Model 1.

A slightly modified version of the nucleon- and pion-nucleus scaling model[2]) (Model 1) has been included in HETC. It was observed from comparisons with experimental data that scaling Model 1 overestimated the number of high-energy particles of the same type as the incident particle emitted from the nucleus in the forward direction. Many of these particles originate from peripheral collisions in which the incident particle transfers a small amount of energy to a nucleon within the nucleus and then leaves the nucleus without further collision. To allow a more favorable comparison

*The authors wish to thank Dr. T. W. Armstrong of the Oak Ridge National Laboratory for the use of the transport code HETC previous to its publication. Comparisons of HETC calculations with experimental results are given in ref.[4]).

between calculated and experimental data, modifications to scaling Model 1 were required. A description of the changes and comparisons between the modified and original nucleon-nucleus scaling model are given in ref.[8]).

Nonelastic nucleon- and pion-proton collisions for energies < 3 GeV are accounted for by the use of the isobar model of Sternheimer and Lindenbaum[9]), as developed by Bertini[5]).

The nucleon- and pion-nucleon scaling model (Model 2) was used to obtain the differential particle yields at energies > 3 GeV for nucleon and pion collisions with hydrogen. The mechanics of this model are based in part on the procedures used with Model 1[2]). A brief description of scaling Model 2 is given in ref.[8]). Although Model 2 met with limited success, the sensitivity of the results presented here is not highly dependent on the accuracy of this phase of the calculation. At energies > 3 GeV, the fraction of collisions with hydrogen is small.

In the previous calculation[1]), the nucleon and pion spectra at energies > 3 GeV emitted from the Be target were obtained using the phenomenological fits of Ranft and Borak[10]). Also, these particles were assumed to enter the wall parallel to the tunnel axis. In this calculation, these spectra are obtained using the nucleon- and pion-nucleus scaling Model 1, and the small-angle approximation is no longer needed. In addition, in the previous work[1]) high-energy collisions (> 3 GeV) occurring at the edge of the tunnel were accounted for using the straightahead approximation for emerging particles with energies > 3 GeV in combination with a normal 3-GeV particle nucleus collision to handle the remaining low-energy particles. Since the data reported here do not require these simplifications, by using HETC the calculations represent a more accurate description of the physical processes.

The transport of low-energy neutrons (< 15 MeV) was accomplished using the O5R Monte Carlo transport code[11]). This code relies on experimentally determined neutron cross sections for predicting elastic and nonelastic neutron-nucleus collisions. Nonelastic neutron-nucleus collisions are handled with the evaporation code[7]).

If the neutron, proton, and pion fluxes are known, the induced activity in the soil may be calculated from the expression

$$A(\rho,z,t_i,t_s,I) = \sum_k A_k(\rho,z,t_i,t_s,I) = \sum_k P_k(\rho,z)(1 - e^{-\lambda_k t_i})\, e^{-\lambda_k t_s}$$

$$P_k(\rho,z) = \sum_i \sum_j I \int_{E_{th_{kji}}}^{E_{max}} dE_i\ \eta_j\ \sigma_{ijk}(E_i)\ \Phi_i(\rho,z,E_i)\ , \tag{1}$$

where

$A(\rho,z,t_i,t_s,I)$ = the total activity at ρ,z for an irradiation time of t_i and a time after shutdown of t_s when there are I 500-GeV protons incident per second;

$A_k(\rho,z,t_i,t_s,I)$ = the partial activity of the kth-type of radioactive nucleus;

$P_k(\rho,z)$ = the production rate of the kth-type radioactive nucleus for I 500-GeV protons incident per second;

λ_k = the decay rate of the kth-type nucleus;

$E_{th_{kji}}$ = the threshold energy for producing the kth-type nuclei from a nucleus of type j by a particle of type i;

η_j = the number density nuclei of type j;

$\sigma_{ijk}(E_i)$ = the microscopic cross section at energy E_i for the production of a nucleus of type k when a particle of type i collides with a target nucleus of type j;

$\Phi_i(\rho,z,E_i)$ = the omnidirectional flux per unit energy of particles of type i due to one 500-GeV proton incident per second.

The activity in the soil was calculated from Eq. 1 using proton, neutron, and charged-pion fluxes. The cross-section data used in calculating the activity are taken from refs.[12-24]). The induced activity arising from the charged pions was calculated using the same cross sections as for protons. All radioactive nuclei which can be produced from the elements in the soil and which have half-lives > one day were considered. A list of these nuclei, along with their half-lives, is given in Table II. It should be noted that several nuclei (see Table II) which have half-lives < one day can decay into long-lived nuclei ($\tau_{\frac{1}{2}}$ > 1 day). The production of these nuclei was also considered. It was assumed that these shorter lived nuclei when produced decayed instantaneously into the longer lived nuclei. Some of the long-lived nuclei decay into nonstable elements. In calculating the induced activity produced by these nuclei, the subsequent secondary decays have not been included. Some of the listed nuclei, indicated by *, have two decay rates. Because of the method in which some of the production cross

TABLE II

Radioactive Nuclei (z < 28) with Half-Lives > 1 Day

Element	Half-Life (years)	
^{3}H	1.23×10^{1}	
^{7}Be	1.47×10^{-1}	
^{10}Be	2.70×10^{6}	
^{14}C	5.77×10^{3}	
^{22}Na	2.58×10^{0}	
* ^{26}Al	7.40×10^{5}	$(^{26}Si \xrightarrow{2\ sec} {}^{26}Al + \beta^{+})$
^{32}Si	7.00×10^{2}	$^{32}Si \longrightarrow {}^{32}P + \beta^{-}$
^{32}P	3.92×10^{-2}	
^{33}P	6.85×10^{-2}	
^{35}S	2.37×10^{-1}	
^{36}Cl	3.00×10^{5}	
^{37}Ar	9.39×10^{-2}	$(^{37}K \xrightarrow{1.2\ sec} {}^{37}Ar + \beta^{+})$
^{39}Ar	2.60×10^{2}	$(^{39}Cl \xrightarrow{55.5\ min} {}^{39}Ar + \beta^{-})$
^{42}Ar	3.30×10^{1}	$^{42}Ar \longrightarrow {}^{42}K + \beta^{-} \xrightarrow{12.4\ h} {}^{42}Ca + 2\beta^{-}$
^{40}K	1.30×10^{9}	
^{41}Ca	1.10×10^{5}	$(^{41}S \xrightarrow{0.87\ sec} {}^{41}Ca + \beta^{+})$
^{45}Ca	4.52×10^{-1}	$(^{45}K \xrightarrow{20\ min} {}^{45}Ca + \beta^{-})$
^{47}Ca	1.29×10^{-2}	
* ^{44}Sc	6.57×10^{-3}	$^{47}Ca \longrightarrow {}^{47}Sc + \beta^{-}$
* ^{46}Sc	2.30×10^{-1}	
^{47}Sc	9.31×10^{-3}	
^{48}Sc	5.02×10^{-3}	$^{44}Ti + e^{-} \longrightarrow {}^{44}Sc$
^{44}Ti	4.70×10^{1}	
^{48}V	4.41×10^{-2}	$(^{48}Cr + e^{-} \xrightarrow{23\ h} {}^{48}V)$
^{49}V	9.04×10^{-1}	$(^{49}Cr \xrightarrow{42\ min} {}^{49}V + \beta^{+})$
^{51}Cr	7.61×10^{-2}	$(^{51}Mn \xrightarrow{45\ min} {}^{51}Cr + \beta^{+})$
* ^{52}Mn	1.53×10^{-2}	$(^{52}Fe \xrightarrow{8\ h} {}^{52}Mn + \beta^{+})$
^{53}Mn	2.00×10^{6}	$(^{53}Fe \xrightarrow{9\ min} {}^{53}Mn + \beta^{+})$
^{54}Mn	7.97×10^{-1}	
^{55}Fe	2.70×10^{0}	$(^{55}Co \xrightarrow{18\ h} {}^{55}Fe + \beta^{+})$
^{59}Fe	1.23×10^{-1}	
^{56}Co	2.19×10^{-1}	
^{57}Co	7.31×10^{-1}	
* ^{58}Co	1.97×10^{-1}	

*Indicates elements that have two decay rates.

sections for these elements were calculated[12,16]), it was not possible to distinguish between the isomeric states formed. It was therefore assumed that the cross sections obtained represented the isomeric state which has the greater half-life.

In these calculations, 70% of the incident 500-GeV protons were allowed to interact in the Be target. It was assumed that the target was sufficiently thin (one nuclear mean free path at 500 GeV) that attenuation of secondary particles produced in the target could be neglected. The remaining 30% of the incident beam was allowed to pass undeflected through the target and strike the wall at the end of the tunnel at $z = 600$ m and $\rho = 0$ cm. Unless otherwise stated, all of the results given below are for a time average proton beam current of 10^{13} protons per second, an irradiation time of 25 years and for a time after shutdown of one month.

3. RESULTS AND DISCUSSION

The omnidirectional neutron, proton, and charged-pion flux distributions at the end of the target tunnel are shown in Fig. 2 as a function of particle energy. These distributions were obtained by averaging the flux over the axial coordinates between $600 \leq z \leq 601$ m and over the radial interval between $0 \leq \rho \leq 0.229$ m. The flux distributions are normalized to one incident 500-GeV proton per second. Figure 3 gives the induced activity as a function of depth in the tunnel ($-50 \leq z \leq 600$ m) for several radial intervals. Figure 4 gives the induced activity as a function of depth at the end of the target tunnel (for $600 \leq z \leq 612$ m) for various radial intervals.

The distributions given in Fig. 3 show peaks in the depth interval between 50 and 100 m beyond the target location. The location and magnitude

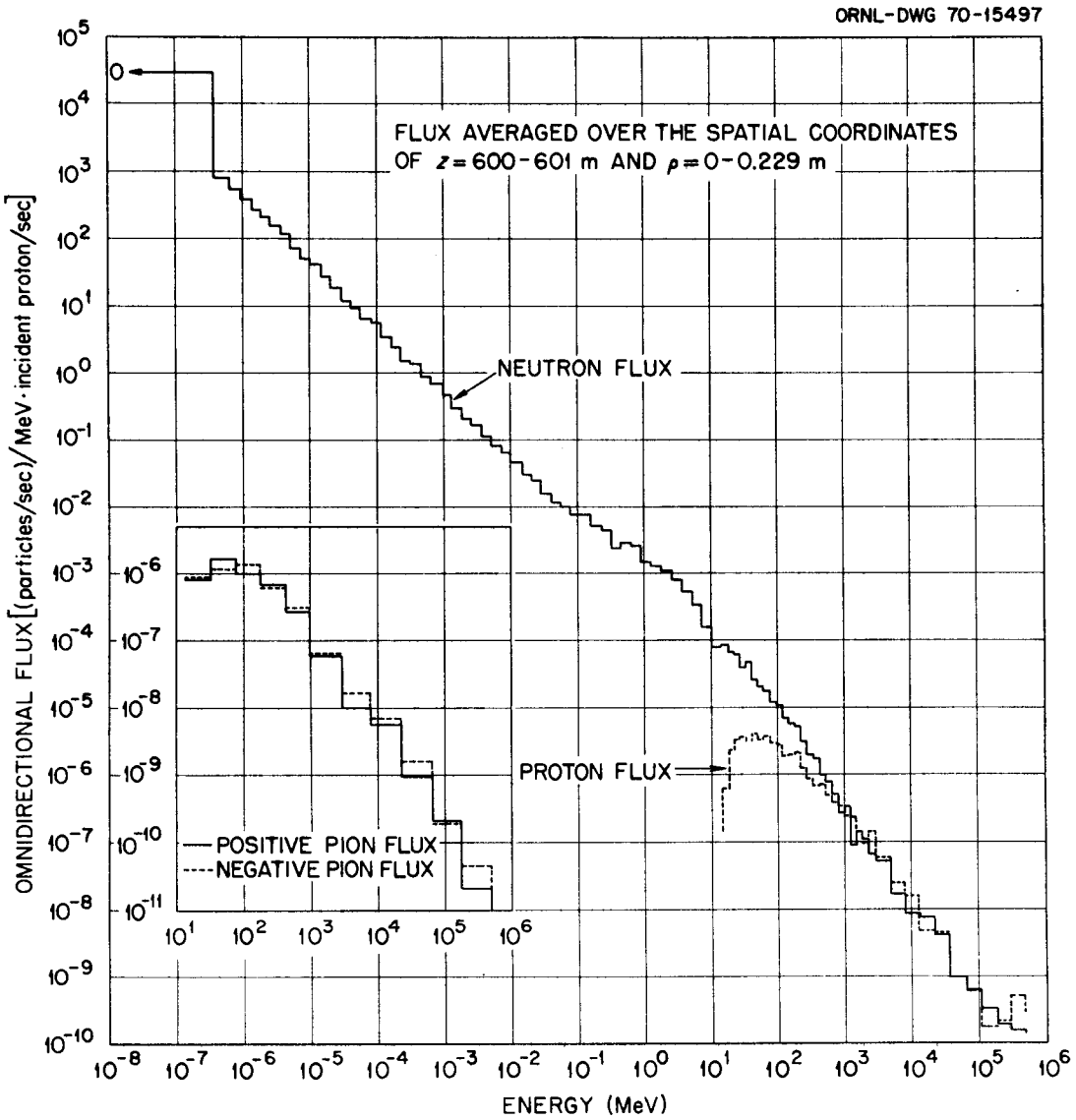

Fig. 2. Neutron, Proton, and Pion Flux Distributions at the End of the Target Tunnel vs Nucleon Energy.

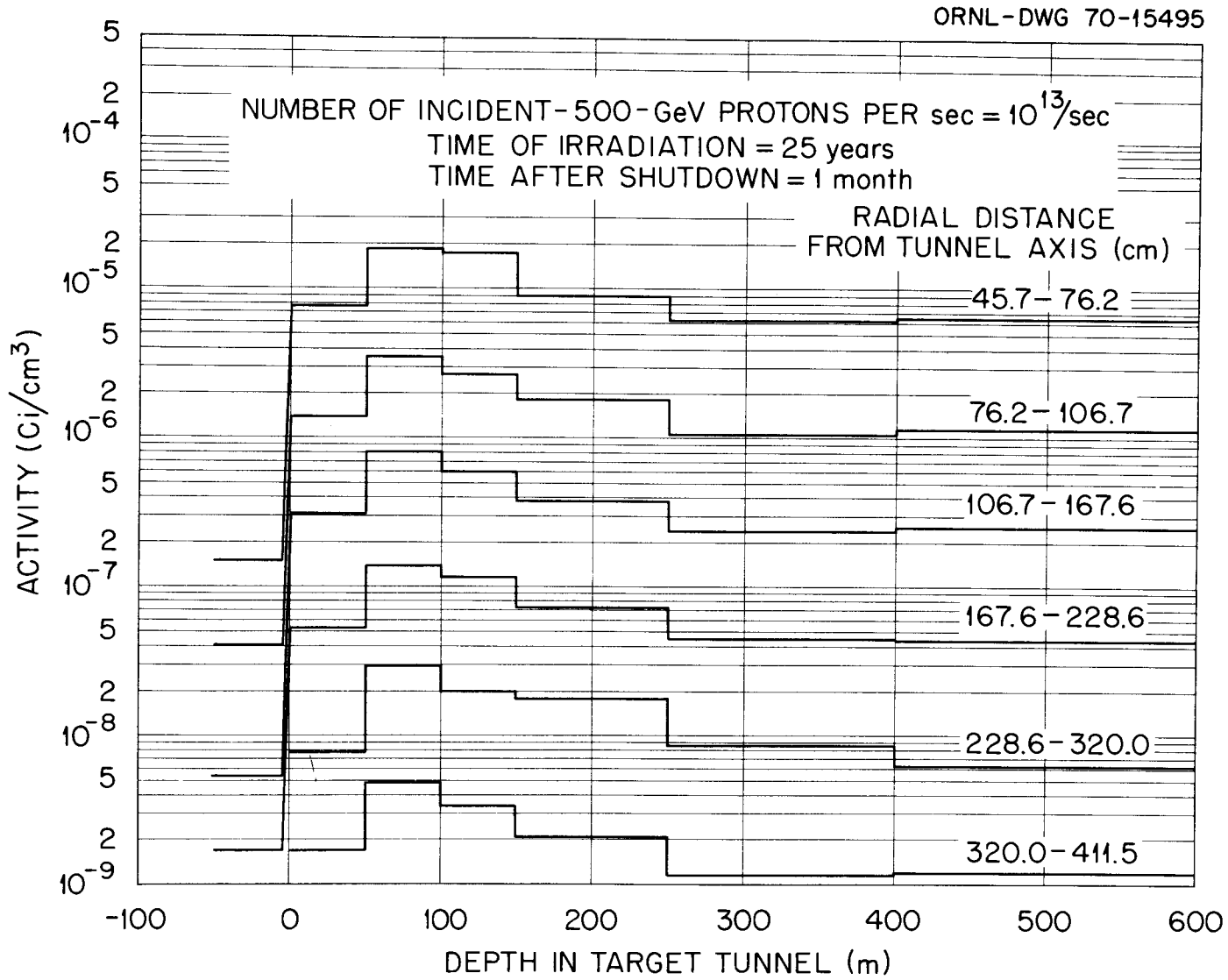

Fig. 3. Induced Activity vs Depth in the Target Tunnel.

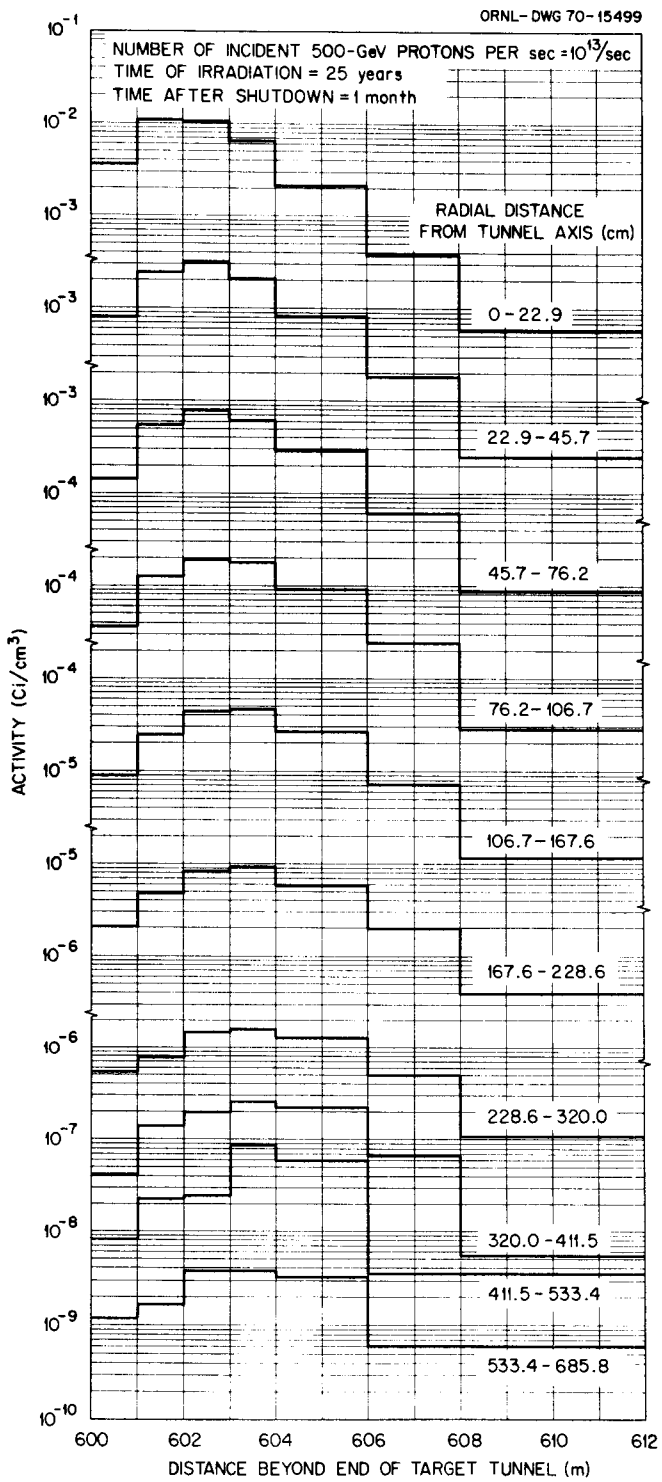

Fig. 4. Induced Activity vs Depth at the End of the Target Tunnel.

of these peaks agree approximately with those obtained in a previous paper[1]) for corresponding radial intervals. Quantitative comparisons between the present and previous calculations are not possible due to geometry and material changes. The data presented here do not, however, show as rapid a decrease in activity with increasing z as was previously obtained. The flatter activity with increasing z arises from the calculational model used and from those particles that escape from the tunnel wall* and reenter the soil at a new location. There is also some contribution to the activity near the end of the tunnel from particles scattered in the backward direction from the end of the tunnel ($\sim$ 15%).† These effects tend to flatten the activity distributions.

At the end of the tunnel, the soil activity distributions, shown in Fig. 4, are approximately an order of magnitude greater than those obtained for the region along the tunnel wall for the same radial intervals shown in Fig. 3. This increase is due mainly to the contributions to the activity induced by the fraction ($\sim$ 30%) of 500-GeV protons that pass through the Be target and strike the soil at the end of the tunnel. The resulting cascade of secondary particles produces a large localized activity. The peak in the activity at the end of the tunnel is further increased by those particles that escape from the tunnel wall at angles small enough to permit entry into the end surface and from those secondary particles that emerge from the Be target at small angles and also impinge on the end wall. This effect is shown in Fig. 5 where the activity as a function of the axial position z along the tunnel for the radial interval $45.7 \leq \rho \leq 76.2$ cm is given.

*In Ref. 1, only particles with energy < 3 GeV could escape from the tunnel surface.

†In Ref. 1, the tunnel was of infinite extent in positive and negative z directions.

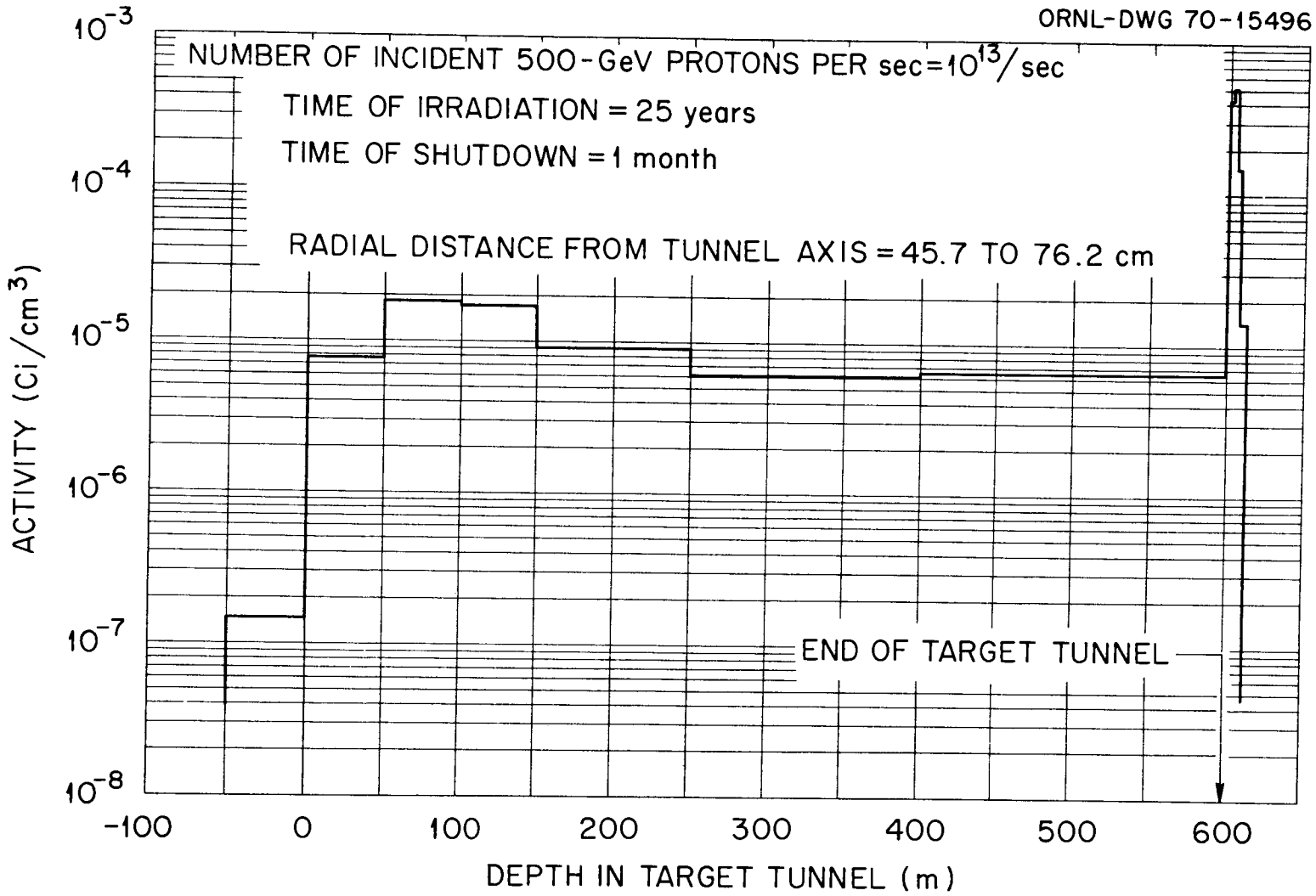

Fig. 5. Composite Induced Activity Distribution in the Target Tunnel and at the End of the Tunnel.

The radial dependence of the induced activity is shown in Fig. 6. Values of constant activity with z and ρ can be inferred from these distributions.

Tables III and IV give the contribution to the total activity of each of the 34 nuclides listed in Table II for the depth intervals of $50 \leq z \leq 100$ m and $602 \leq z \leq 603$ m, respectively, and for several radial intervals. The decay of the major contributors to the activity for the time after shutdown in years at the spatial location $602 \leq z \leq 603$ m and $0 \leq \rho \leq 0.229$ m is shown in Fig. 7. Comparison between this curve and the one obtained previously shows similar behavior[1]).

The total integrated activity as a function of z is given in Fig. 8. These data were obtained from the integral

$$A(z) = \int_{\text{all } v<z} A(v)dv$$

where v is the volume element. For an irradiation time of 25 years and a time-averaged beam current of 10^{13} protons per second, the total activity following one month of shutdown is 2.62×10^4 curies.

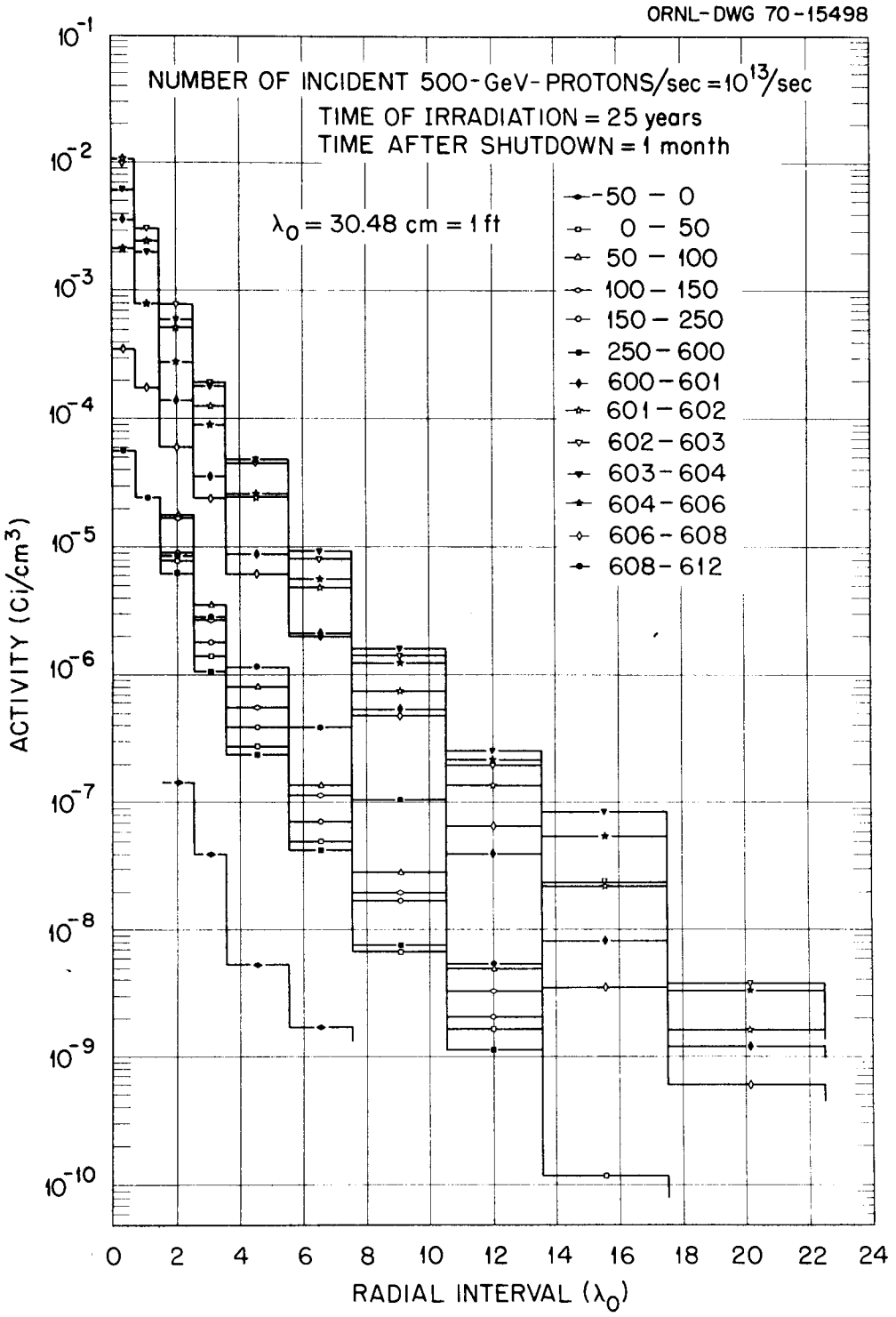

Fig. 6. Induced Activity vs Radial Distance from the Target Tunnel Axis.

TABLE III

ACTIVITY DUE TO INDIVIDUAL NUCLIDES AVERAGED OVER THE INTERVALS Z = 50 M TO Z = 100 M AND OVER THE INDICATED RADIALS INTERVALS

NUMBER OF INCIDENT 500-GEV PROTONS PER SECOND = 1.0E13
TIME OF IRRADIATION = 25 YEARS
TIME AFTER SHUTDOWN = 1 MONTH

ACTIVITY (CI/CM**3)

ELEMENT	RHO = 45.7 TO 76.2 CM	RHO = 76.2 TO 106.7 CM	RHO = 106.7 TO 167.6 CM	RHO = 167.6 TO 228.6 CM	RHO = 228.6 TO 320.0 CM	RHO = 320.0 TO 411.5 CM
H(3)	6.76E-06	5.96E-07	9.60E-08	1.38E-08	2.72E-09	4.40E-10
BE(7)	1.15E-06	8.28E-08	1.15E-08	1.42E-09	2.76E-10	4.86E-11
BE(10)	2.78E-12	4.71E-13	1.11E-13	2.15E-14	4.51E-15	6.85E-16
C(14)	7.56E-09	1.86E-09	4.64E-10	8.96E-11	1.92E-11	2.99E-12
NA(22)	2.57E-06	5.26E-07	1.28E-07	2.54E-08	5.35E-09	8.07E-10
AL(26)	2.30E-10	4.88E-11	1.21E-11	2.34E-12	4.88E-13	9.12E-14
SI(32)	4.38E-11	4.57E-12	8.03E-13	1.16E-13	1.82E-14	1.37E-15
P(32)	5.65E-08	9.09E-09	2.03E-09	3.82E-10	7.79E-11	1.09E-11
P(33)	1.43E-08	2.66E-09	6.22E-10	1.21E-10	2.57E-11	3.70E-12
S(35)	7.53E-08	1.61E-08	3.93E-09	7.85E-10	1.72E-10	2.62E-11
CL(36)	4.81E-11	1.06E-11	2.60E-12	4.96E-13	1.08E-13	1.74E-14
AR(37)	2.47E-06	6.63E-07	1.62E-07	2.40E-08	5.92E-09	1.13E-09
AR(39)	2.58E-08	6.95E-09	1.72E-09	2.81E-10	6.43E-11	1.33E-11
AR(42)	1.04E-08	2.45E-09	6.23E-10	1.23E-10	2.66E-11	4.15E-12
K(40)	1.56E-13	5.74E-14	1.38E-14	2.12E-15	4.60E-16	7.78E-17
CA(41)	1.53E-09	6.38E-10	1.51E-10	2.46E-11	4.91E-12	7.50E-13
CA(45)	5.87E-07	2.46E-07	5.82E-08	9.47E-09	1.89E-09	2.82E-10
CA(47)	9.97E-11	2.71E-11	7.14E-12	1.35E-12	2.78E-13	5.58E-14
SC(44)	7.75E-12	8.41E-13	1.47E-13	2.11E-14	3.43E-15	2.77E-16
SC(46)	1.78E-08	2.58E-09	5.29E-10	8.77E-11	1.43E-11	1.01E-12
SC(47)	2.23E-11	3.50E-12	7.16E-13	1.16E-13	1.87E-14	1.02E-15
SC(48)	5.23E-14	6.59E-15	1.08E-15	1.51E-16	3.16E-17	4.77E-18
TI(44)	1.38E-09	1.03E-10	1.36E-11	1.16E-12	1.58E-13	9.10E-15
V(48)	1.90E-08	3.51E-09	7.85E-10	1.48E-10	2.65E-11	2.97E-12
V(49)	1.38E-07	2.30E-08	5.05E-09	9.35E-10	1.79E-10	2.12E-11
CR(51)	1.22E-07	2.47E-08	5.94E-09	1.18E-09	2.58E-10	3.97E-11
MN(52)	4.76E-09	9.85E-10	2.39E-10	4.76E-11	1.03E-11	1.53E-12
MN(53)	5.62E-12	1.36E-12	3.47E-13	6.83E-14	1.44E-14	2.32E-15
MN(54)	5.11E-07	1.22E-07	3.05E-08	5.74E-09	1.26E-09	2.14E-10
FE(55)	3.50E-06	1.30E-06	3.14E-07	5.33E-08	1.06E-08	1.69E-09
FE(59)	3.79E-08	1.59E-08	3.77E-09	6.14E-10	1.23E-10	1.82E-11
CO(56)	2.43E-08	2.75E-09	4.45E-10	8.54E-11	1.45E-11	1.33E-12
CO(57)	6.57E-10	7.44E-11	1.21E-11	2.31E-12	3.92E-13	3.61E-14
CO(58)	7.57E-11	8.69E-12	1.42E-12	2.73E-13	4.64E-14	4.27E-15
TOTAL	1.82E-05	3.65E-06	8.27E-07	1.38E-07	2.91E-08	4.76E-09

TABLE IV

ACTIVITY DUE TO INDIVIDUAL NUCLIDES AVERAGED OVER THE INTERVALS Z = 602 M TO Z = 603 M
AND OVER THE INDICATED RADIALS INTERVALS

NUMBER OF INCIDENT 500-GEV PROTONS PER SECOND = 1.0E13
TIME OF IRRADIATION = 25 YEARS
TIME AFTER SHUTDOWN = 1 MONTH

ACTIVITY
(CI/CM**3)

ELEMENT	RHO = 0.0 TO 22.9 CM	RHO = 22.9 TO 45.7 CM	RHO = 45.7 TO 76.2 CM	RHO = 76.2 TO 106.7 CM	RHO = 106.7 TO 167.6 CM	RHO = 167.6 TO 228.6 CM	RHO = 228.6 TO 320.0 CM	RHO = 320.0 TO 411.5 CM
H(3)	4.21E-03	8.57E-04	1.44E-04	2.24E-05	4.57E-06	7.80E-07	1.59E-07	1.64E-08
BE(7)	7.11E-04	1.38E-04	2.13E-05	2.77E-06	5.16E-07	8.15E-08	1.72E-08	1.48E-09
BE(10)	1.57E-09	4.04E-10	1.02E-10	2.59E-11	6.52E-12	1.27E-12	2.65E-13	3.07E-14
C(14)	3.91E-06	1.26E-06	3.87E-07	1.09E-07	2.81E-08	5.39E-09	1.07E-09	1.40E-10
NA(22)	1.39E-03	3.98E-04	1.12E-04	2.95E-05	7.55E-06	1.46E-06	3.01E-07	3.42E-08
AL(26)	1.22E-07	3.63E-08	1.04E-08	2.93E-09	7.38E-10	1.46E-10	2.95E-11	3.46E-12
SI(32)	2.67E-08	5.70E-09	1.06E-09	1.73E-10	3.72E-11	5.99E-12	1.00E-12	7.94E-14
P(32)	3.28E-05	8.26E-06	1.98E-06	4.50E-07	1.07E-07	2.06E-08	4.28E-09	4.57E-10
P(33)	7.90E-06	2.16E-06	5.70E-07	1.39E-07	3.48E-08	6.64E-09	1.36E-09	1.53E-10
S(35)	3.89E-05	1.18E-05	3.41E-06	8.93E-07	2.29E-07	4.41E-08	9.11E-09	1.11E-09
CL(36)	2.55E-08	7.74E-09	2.23E-09	5.96E-10	1.52E-10	2.92E-11	5.95E-12	7.49E-13
AR(37)	1.36E-03	4.70E-04	1.36E-04	3.52E-05	8.50E-06	1.60E-06	2.78E-07	4.05E-08
AR(39)	1.35E-05	4.72E-06	1.38E-06	3.89E-07	9.71E-08	1.86E-08	3.57E-09	5.54E-10
AR(42)	5.28E-06	1.67E-06	5.25E-07	1.48E-07	3.89E-08	7.55E-09	1.56E-09	1.76E-10
K(40)	8.52E-11	3.81E-11	1.18E-11	3.13E-12	6.91E-13	1.30E-13	1.91E-14	3.07E-15
CA(41)	8.25E-07	4.08E-07	1.32E-07	3.54E-08	7.60E-09	1.43E-09	1.97E-10	3.31E-11
CA(45)	3.14E-04	1.57E-04	5.08E-05	1.36E-05	2.92E-06	5.50E-07	7.58E-08	1.27E-08
CA(47)	4.80E-08	1.78E-08	5.76E-09	1.75E-09	4.47E-10	9.15E-11	1.70E-11	2.17E-12
SC(44)	4.77E-09	1.04E-09	1.91E-10	3.14E-11	6.59E-12	1.08E-12	1.94E-13	1.55E-14
SC(46)	1.04E-05	2.50E-06	5.71E-07	1.17E-07	2.57E-08	4.33E-09	8.63E-10	5.96E-11
SC(47)	1.26E-08	3.18E-09	7.57E-10	1.58E-10	3.42E-11	5.48E-12	1.06E-12	7.41E-14
SC(48)	3.15E-11	7.36E-12	1.53E-12	2.56E-13	5.05E-14	8.31E-15	1.67E-15	1.99E-16
TI(44)	8.89E-07	1.76E-07	2.48E-08	2.59E-09	4.50E-10	6.35E-11	8.30E-12	6.17E-13
V(48)	1.10E-05	2.93E-06	7.32E-07	1.76E-07	4.03E-08	7.70E-09	1.61E-09	1.34E-10
V(49)	7.81E-05	2.04E-05	4.94E-06	1.13E-06	2.63E-07	4.84E-08	1.01E-08	9.61E-10
CR(51)	6.60E-05	1.91E-05	5.25E-06	1.34E-06	3.37E-07	6.51E-08	1.33E-08	1.64E-09
MN(52)	2.56E-06	7.44E-07	2.09E-07	5.45E-08	1.39E-08	2.69E-09	5.55E-10	6.48E-11
MN(53)	2.84E-09	9.12E-10	2.91E-10	8.36E-11	2.20E-11	4.25E-12	8.79E-13	1.01E-13
MN(54)	2.63E-04	8.40E-05	2.56E-05	7.17E-06	1.85E-06	3.58E-07	7.24E-08	8.83E-09
FE(55)	1.84E-03	8.43E-04	2.71E-04	7.41E-05	1.66E-05	3.17E-06	4.81E-07	7.76E-08
FE(59)	2.03E-05	1.02E-05	3.30E-06	8.83E-07	1.89E-07	3.57E-08	4.91E-09	8.21E-10
CO(56)	1.73E-05	3.46E-06	7.24E-07	1.39E-07	1.40E-08	1.45E-09	3.49E-10	0.0
CO(57)	4.70E-07	9.38E-08	1.96E-08	3.76E-09	3.80E-10	3.92E-11	9.45E-12	0.0
CO(58)	5.36E-08	1.07E-08	2.29E-09	4.42E-10	4.46E-11	4.60E-12	1.12E-12	0.0
TOTAL	1.04E-02	3.03E-03	7.84E-04	1.90E-04	4.39E-05	8.27E-06	1.44E-06	1.98E-07

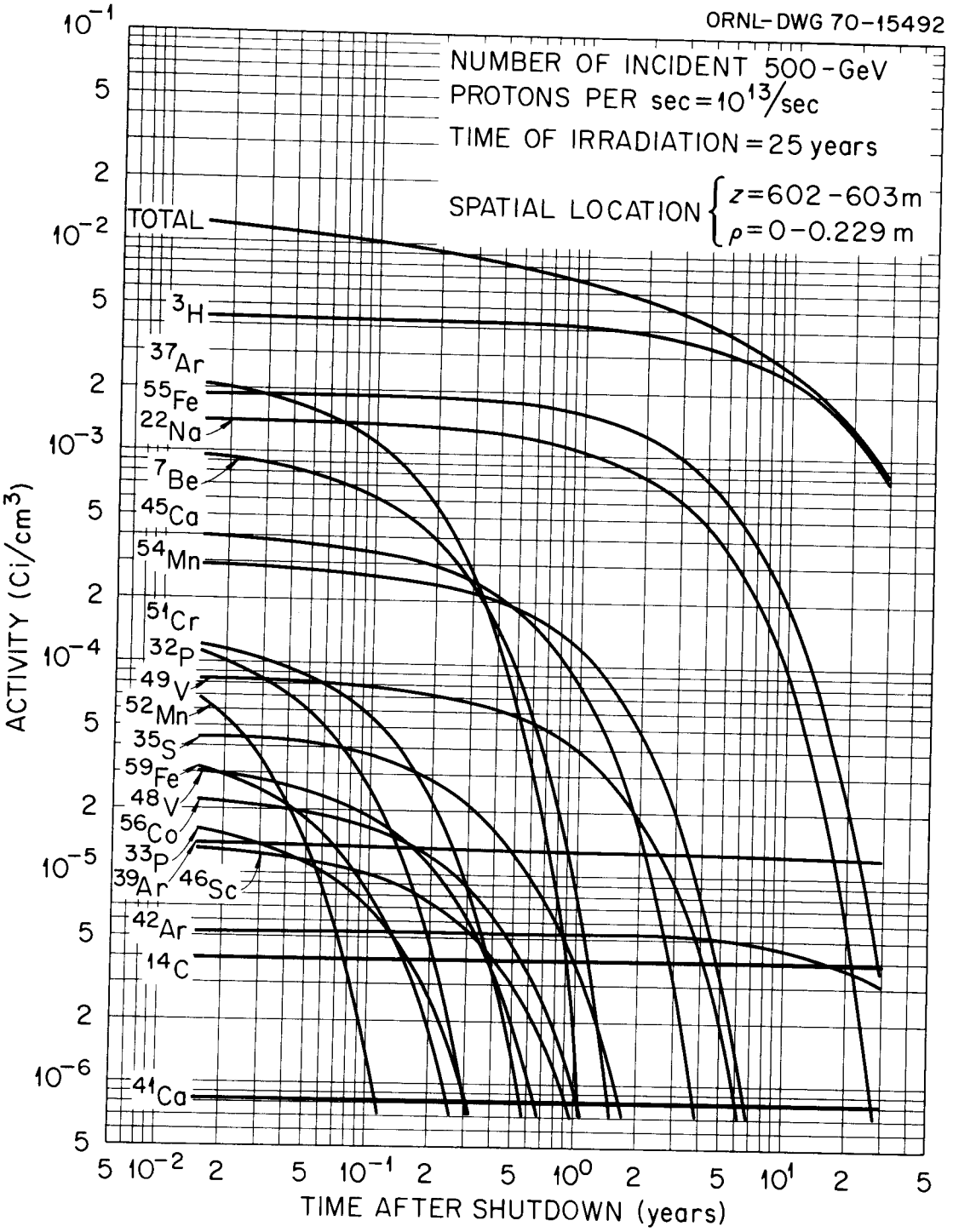

Fig. 7. Induced Activity vs Time After Shutdown (in Years) for the Nuclides Making the Major Contribution to the Activity.

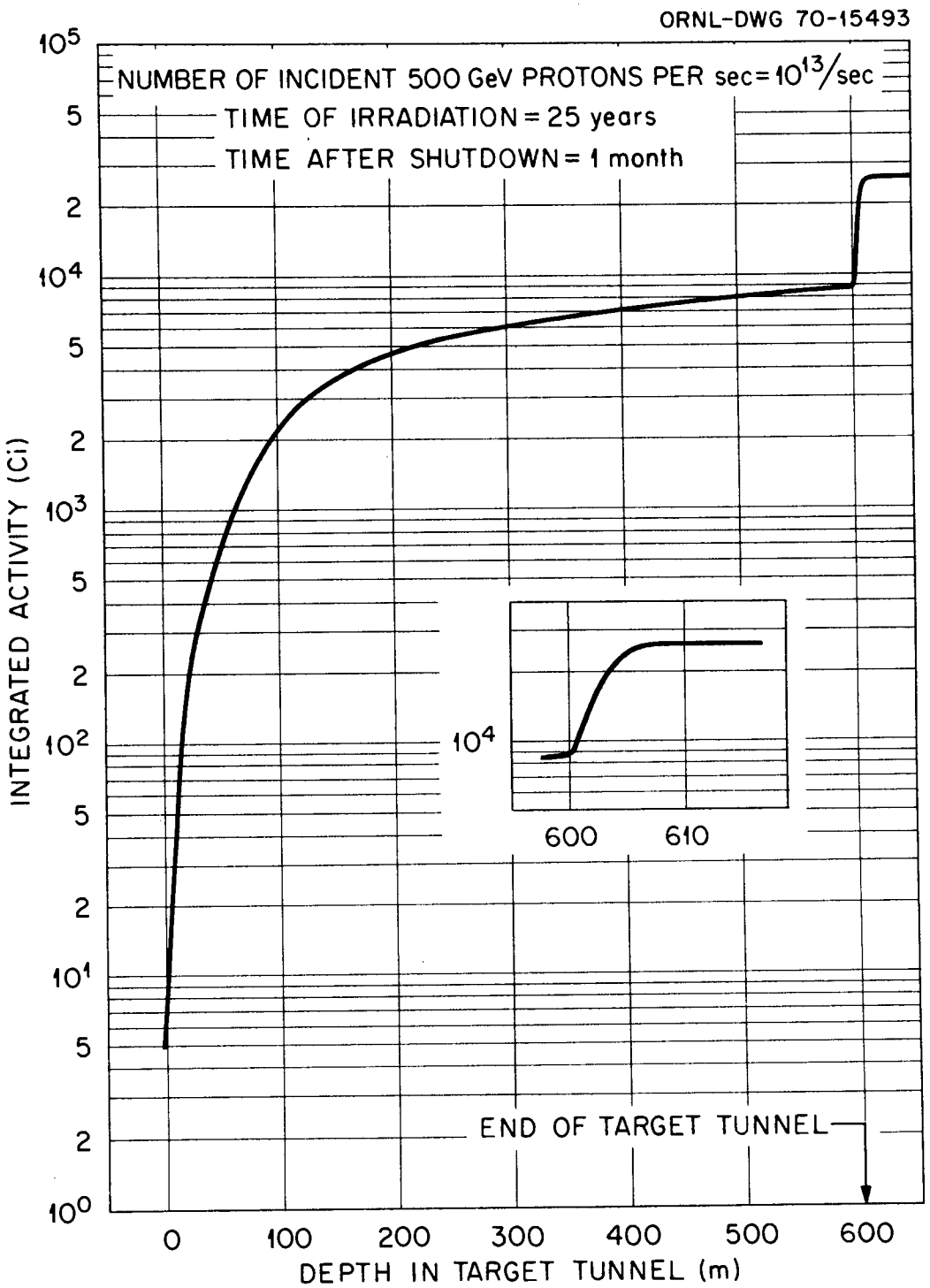

Fig. 8. Integrated Activity vs Depth in the Target Tunnel.

APPENDIX A

To allow a more favorable comparison between calculated and experimental data, the following modification of the nucleon- and pion-nucleus collision model was made. When a high-energy (> 3 GeV) collision occurs where a particle of the same type as the incident particle emerges from the nucleus with energy > 95% of the incident energy and having suffered only "one intranuclear collision," then the event is weighted by 0.2. In order that the total weight remain unity for this collision, a second collision that does not satisfy the above conditions is combined with the collision described above and is assigned a weight of 0.8.

Figures A1 and A2 show the differential proton spectra in the forward direction for 18-GeV protons incident on Be and Pb targets, respectively. These distributions were obtained using the unmodified scaling model described in ref.[2]). The dominant high-energy peak is clearly evident. Figures A3 and A4 give the differential proton spectra for 18-GeV protons on Be and Pb targets, respectively, using the modified scaling model described in the text. For these data, the high-energy peak is reduced by a factor of ~ 5, and better agreement with the experimental data is realized at high energy. The remaining portion of the spectrum is relatively unaltered.

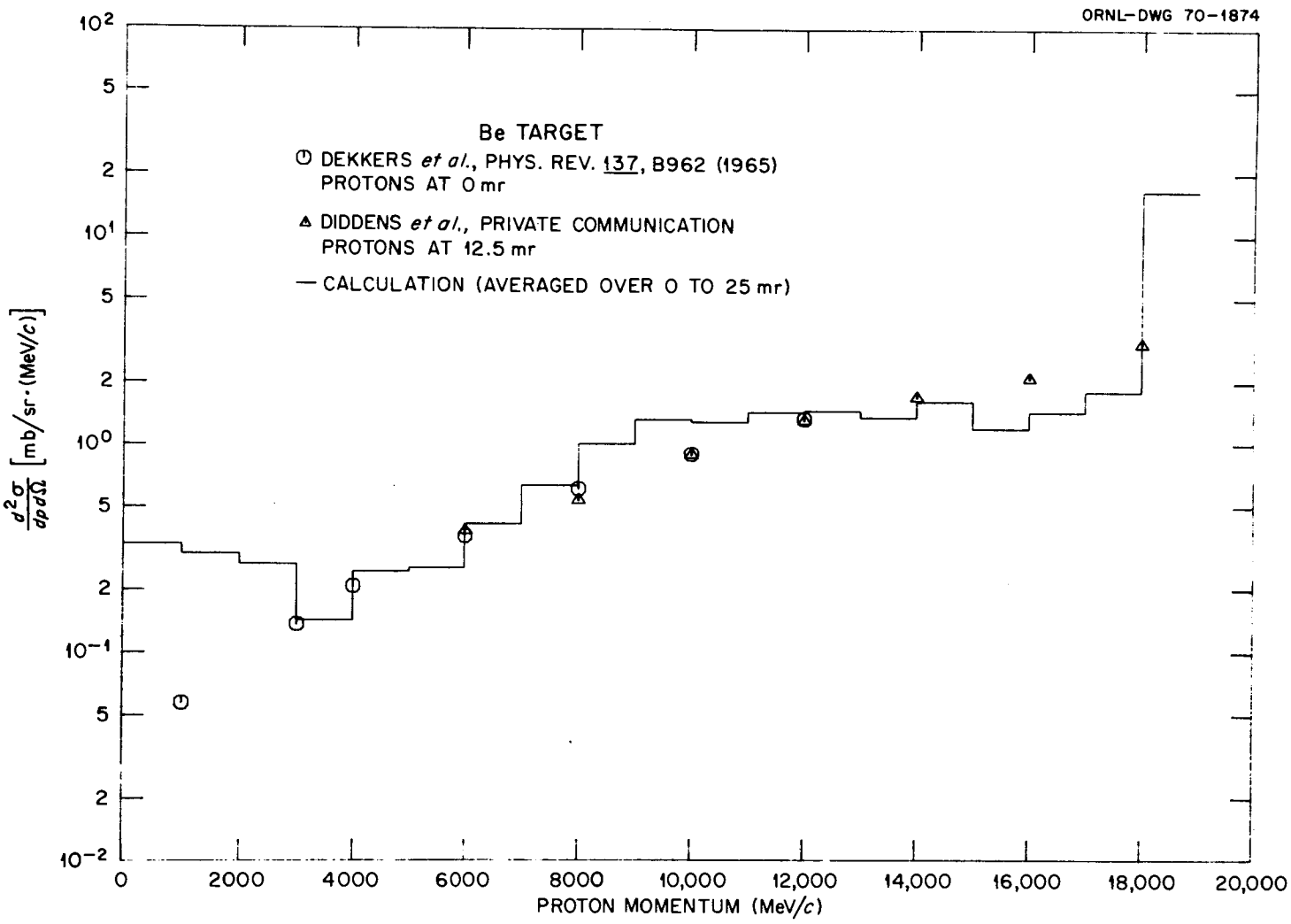

Fig. A1. Differential Cross Sections for the Production of Protons at Very Small Angles from the Collision of 18-GeV Protons with Be Nuclei (from Unmodified Scaling Model).

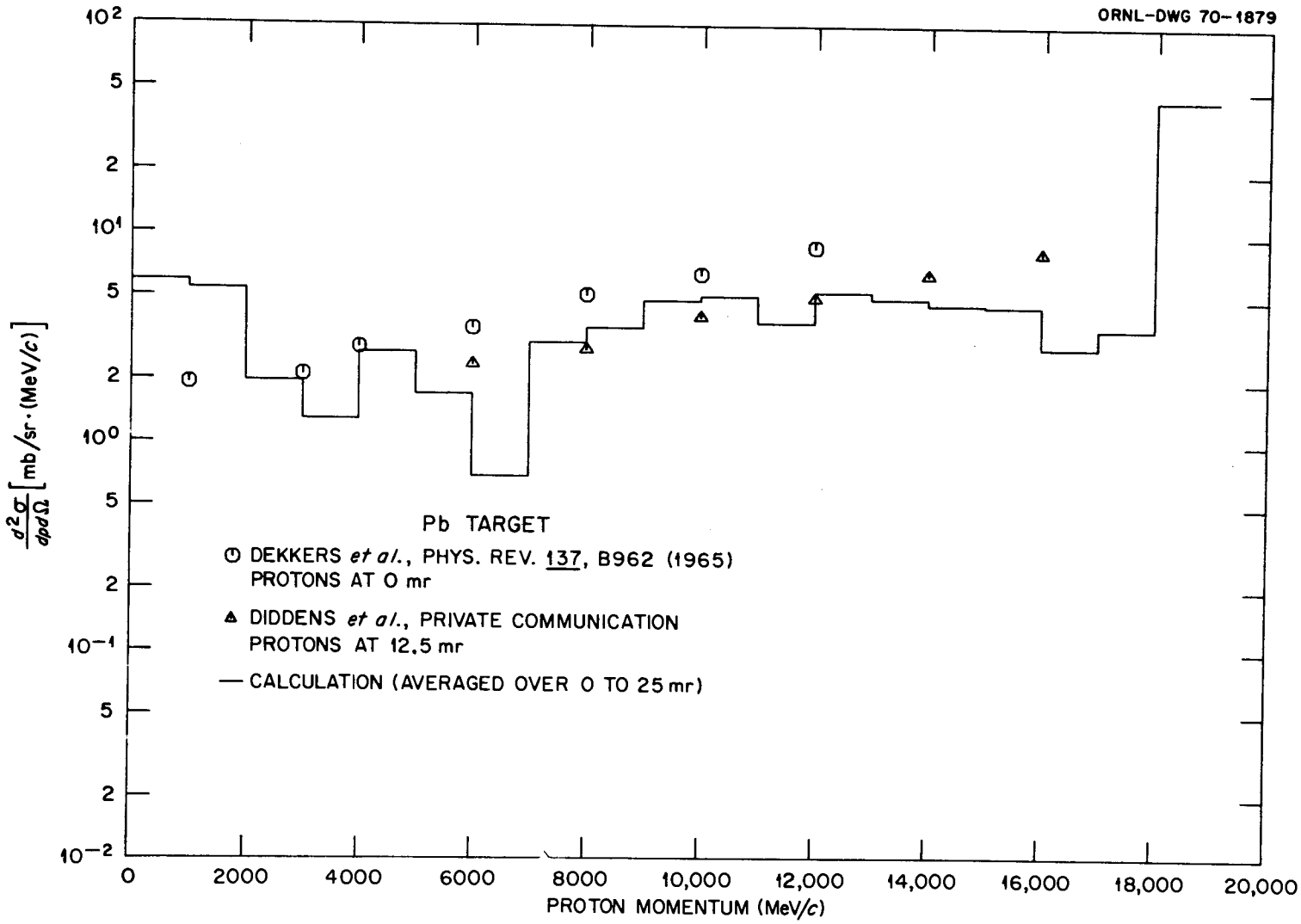

Fig. A2. Differential Cross Sections for the Production of Protons at Very Small Angles from the Collision of 18-GeV Protons with Pb Nuclei (from Unmodified Scaling Model).

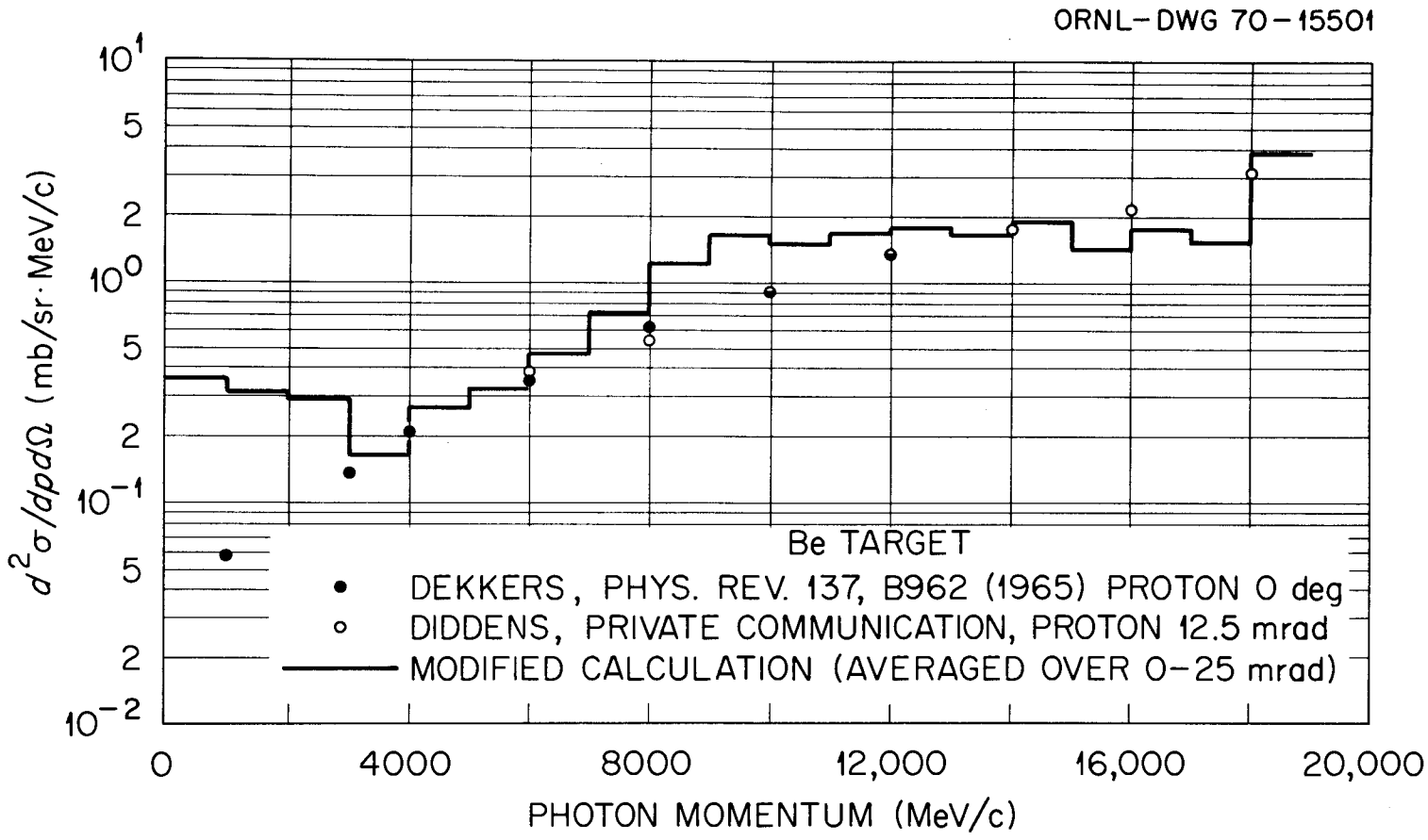

Fig. A3. Differential Cross Sections for the Production of Protons at Very Small Angles from the Collision of 18-GeV Protons with Be Nuclei (from Modified Scaling Model).

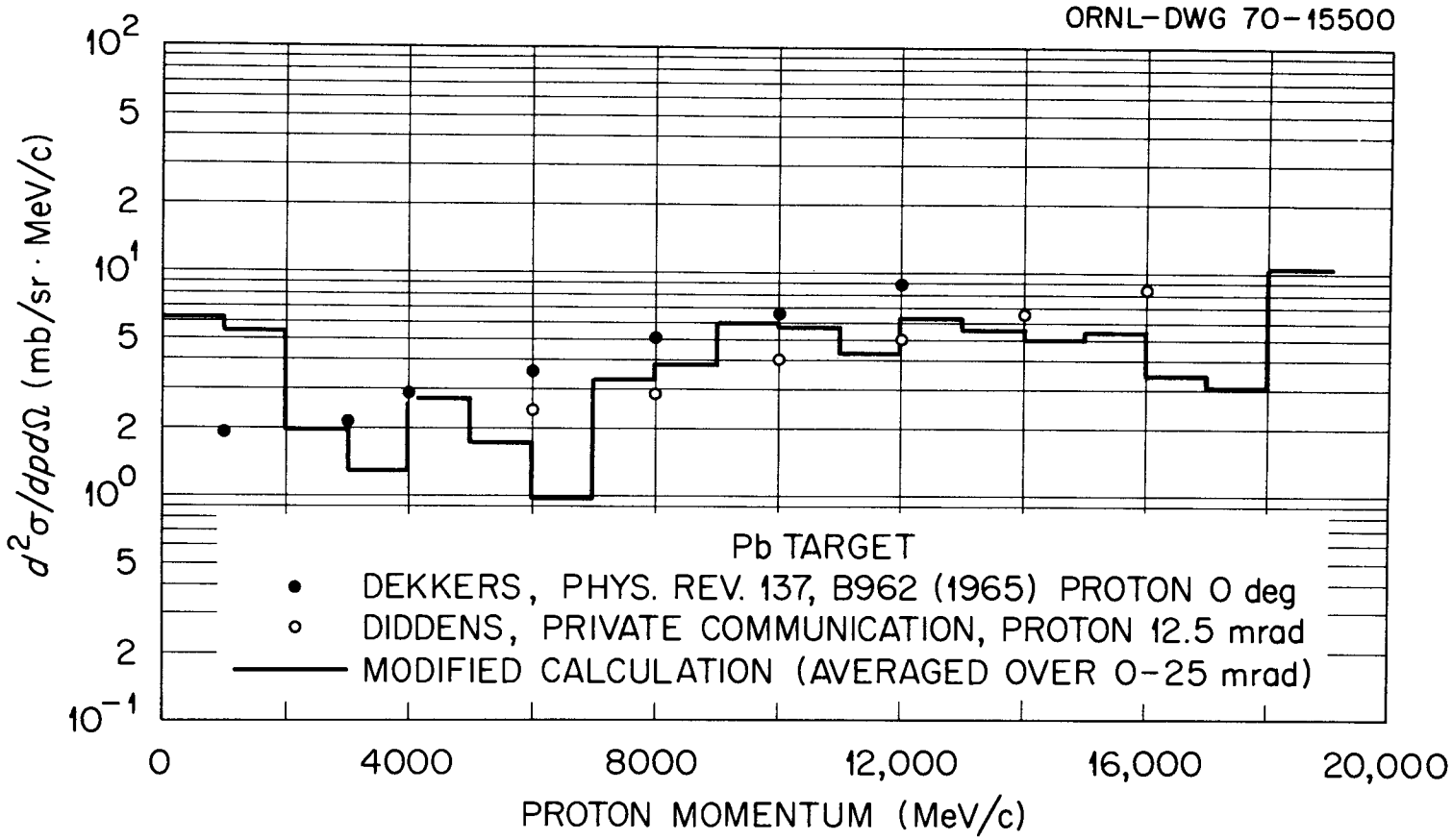

Fig. A4. Differential Cross Sections for the Production of Protons at Very Small Angles from the Collision of 18-GeV Protons with Pb Nuclei (from Modified Scaling Model).

APPENDIX B

To perform high-energy transport calculations in hydrogenous materials, the elastic and nonelastic particle-production cross sections for nucleon- and pion-nucleon collisions are required. These data are available for collisions occurring with energies ≤ 3 GeV (hereinafter called slow collisions) through the use of the isobar model of Sternheimer and Lindenbaum[9,25]. A nucleon- and pion-nucleon scaling model, which was designed to predict the high-energy collision particle-production distributions (hereinafter called fast collisions), is described.

Low-energy collisions provide data on the following parameters:

$\sigma(E_o)$ = the total nonelastic cross section for the collision of a nucleon or pion with laboratory energy E_o;

$\frac{d^2\sigma_i(E_o,\varepsilon,\omega)}{d\varepsilon d\omega}$ = the cross section in the laboratory system for the production of a particle of type i in the total energy range $d\varepsilon$ about ε and in the angular interval $d\omega$ about ω from the collision of a nucleon or pion of energy E_o with a nucleon.* (Neutrons, protons, and charged and neutral pions are all treated.)

ω = the cosine of the angle between the momenta of the incident and emitted particles in the laboratory system.

Since it is more convenient to work with particle energy distributions rather than their double-differential cross sections, the following transformation was used:

$$f_i(\varepsilon\ \omega) = \frac{1}{\sigma(E_o)} \frac{d^2\sigma_i(E_o,\varepsilon,\omega)}{d\varepsilon d\omega} \quad , \tag{2}$$

*The 2π associated with the aximuthal angle is omitted. $d\Omega = 2\pi d\omega$.

where

$f_i(\varepsilon,\omega)$ = the fraction of particles of type i at angle ω with total energy ε.

Since it is also more convenient to scale the particle distributions in the center-of-mass system, transformations from the laboratory system to the center-of-mass system were handled using the Lorentz transformations

$$\varepsilon_c = \gamma(\varepsilon - P\beta\omega) \ , \tag{3}$$

$$P_c \sin \theta_c = P \sin \theta \ , \tag{4}$$

$$\beta = \frac{(E_o^2 + 2E_o M_o)^{\frac{1}{2}}}{E_o + M_o + M_T} \ , \tag{5}$$

$$\gamma = (1 - \beta^2)^{-\frac{1}{2}} \ , \tag{6}$$

where

ε_c, P_c = the total energy and momentum of the particle in the center-of-mass system, respectively,

θ_c = the polar angle with respect to the direction of motion of the incident particle in the center-of-mass system,

M_o, M_T = the rest energies of the incident and struck particles, respectively.

The energy-angle distribution of secondary particles in the center-of-mass system for a particle of type i is obtained from the associated distribution in the laboratory system from the transformation

$$f_{ic}(\varepsilon_c,\omega_c)\ d\varepsilon_c d\omega_c = f_i(\varepsilon,\omega)\ d\varepsilon d\omega \ , \tag{7}$$

where

ω_c = the angle between the emitted and struck particle in the center-of-mass system.

All quantities used in Eqs. 2-7 that refer to a fast collision will be denoted by primes.

In performing the scaling operations, it was assumed that the total nonelastic cross section is independent of the energy of the incident particle; that is, $\sigma(E'_o) = \sigma(E_o)$. It was also postulated[2]) that the energies of the emitted particles from slow and fast collisions were related by

$$\frac{E'_{ci}}{E'_{co}} = \frac{E_{ci}}{E_{co}} , \tag{8}$$

where

E_{co}, E'_{co} = the kinetic energy of the incident particles in the center-of-mass system for the slow and fast collisions, respectively;

E_{ci}, E'_{ci} = the kinetic energies of particles of type i produced by slow and fast collisions, respectively.

The relationship between the momentum of the particles produced through fast and slow collisions is obtained using

$$\omega'_{ci} = \left[1 - \left(\frac{P_{ci}}{P'_{ci}}\right)^{2\sqrt{|\omega_{ci}|}} (1 - \omega_{ci}^2)\right]^{\frac{1}{2}} , \tag{9}$$

where

$$P = (E^2 - M^2)^{\frac{1}{2}} .$$

The sign of ω'_{ci} is taken to be the same as that of ω_{ci}. Equation 9 is similar to the expression used elsewhere[2]) in that when $\omega_{ci} \sim 1$, the transverse momenta between the slow and fast particles remain the same. When $\omega_{ci} \sim 0$, then $\omega'_{ci} \sim \omega_{ci}$.

Equations 8 and 9 relate ε_c' and ω_c' with ε_c and ω_c but do not imply any relation between the distributions $f_{ci}'(\varepsilon_c',\omega_c')$ and $f_{ci}(\varepsilon_c,\omega_c)$. An understanding of the manner in which these distributions are related can be realized by considering conservation of energy in the center-of-mass system. For slow collisions,

$$\varepsilon_{co} + \varepsilon_{cTo} = \sum_{i=p,n,\pi^+,\pi^-,\pi^o} \int \varepsilon_{ci}\, f_{ci}(\varepsilon_{ci},\omega_{ci})d\varepsilon_{ci}d\omega_{ci} \ , \tag{10}$$

where

$\varepsilon_{co},\varepsilon_{cTo}$ = the total energy of the incident and struck particles in the center-of-mass system, respectively,

ε_{ci} = the total energy of the emitted particles of type i in the center-of-mass system.

In nucleon-nucleon collisions with the proton and neutron rest energies taken to be equal, Eq. 10 becomes

$$1 = \sum_{i=n,p} \int \frac{E_{ci}}{2E_{co}} f_{ci}(E_{ci},\omega_{ci})dE_{ci}d\omega_{ci} + \sum_{i=\pi^+,\pi^-,\pi^o} \frac{\varepsilon_{ci}}{2E_{co}} f_{ci}(\varepsilon_{ci},\omega_{ci})d\varepsilon_{ci}d\omega_{ci} \tag{11}$$

since $E_{co} = E_{cTo}$. A similar equation for fast collisions is obtained by the addition of primes to the variables in Eq. 11. Equating the differential quantities for like particles using Eq. 11 for fast and slow particles, the relation for nucleon scaling is

$$\frac{E_{ci}}{E_{co}} f_{ci}(E_{ci},\omega_{ci})dE_{ci}d\omega_{ci} = \frac{E_{ci}'}{E_{co}'} f_{ci}'(E_{ci}',\omega_{ci}')dE_{ci}'d\omega_{ci}' \ , \tag{12}$$

and for pions

$$\frac{\varepsilon_{ci}}{E_{co}} f_{ci}(\varepsilon_{ci},\omega_{ci})d\varepsilon_{ci}d\omega_{ci} = \frac{\varepsilon'_{ci}}{E'_{co}} f'_{ci}(\varepsilon'_{ci},\omega'_{ci})d\varepsilon'_{ci}d\omega'_{ci} \ . \tag{13}$$

Using Eqs. 8 and 12,

$$\nu' = \nu = \int f_{ci}(E_{ci},\omega_{ci})dE_{ci}d\omega_{ci} \ . \tag{14}$$

Equation 14 says that baryons are conserved through the scaling procedure and that they are given a weight of unity. For pions,

$$\nu'_i = \int \left(\frac{E'_{co}}{E_{co}} \times \frac{\varepsilon_{ci}}{\varepsilon'_{ci}}\right) f_{ci}(\varepsilon_{ci},\omega_{ci})d\varepsilon_{ci}d\omega_{ci} \ , \tag{15}$$

and the scaled pions are given a weight of

$$\frac{E'_{co}}{E_{co}} \times \frac{\varepsilon_{ci}}{\varepsilon'_{ci}} \ .$$

Following the scaling to high energy, the energy and momentum components are transformed back to the laboratory system using the Lorentz transformation. From the use of these equations, conservation of energy, but not momentum, is achieved for the center-of-mass system. Transformation to the laboratory system gives results which fail to conserve both energy and momentum. For the cases considered here, an $\sim$ 10% error in energy conservation for particle-particle production > 3 GeV resulted.

To scale when pions are the incident particles, equations similar to those given above are used. The resulting weights are

$$\frac{E_{ci}(E'_{cT} - m_n - m_\pi)}{E'_{ci}(E_{cT} - m_n - m_\pi)}$$

for the nucleons and recoil pions and

$$\frac{\varepsilon_{ci}(E'_{cT} - m_n - m_\pi)}{\varepsilon'_{ci}(E_{cT} - m_n - m_\pi)}$$

for the produced pions, where

m_n = the mass of the nucleon

m_π = the mass of the incident pion

E_{cT}, E'_{cT} = the total energy in the center-of-mass system of the slow and fast collisions, respectively.

Figures B1, B2, and B3 show comparisons between calculated and experimental data for p-p collisions at 19.2 GeV/c. The calculated results are for two different angular distributions of the produced isobars.* These data were obtained by scaling 3-GeV p-p data generated by Bertini's adaptation of the isobar model[25]).

In Figs. B1 and B2 the secondary-proton spectrum for emergent particles at an average laboratory angle of 12.5 and 40 mrad, respectively, is given, and in Fig. B3 the secondary π^+ spectrum for an average laboratory angle of 40 mrad is given.

The agreement between the calculated and experimental[26,27]) results is marginal. The nucleon comparisons show better agreement than those obtained for pions. However, as stated in the text, the results of the calculations are not sensitive to this scaling model since the number of nucleon- and pion-nucleus collisions > 3 GeV is small.

*The angular distributions used in the activity calculations described in the text were obtained from Bertini.

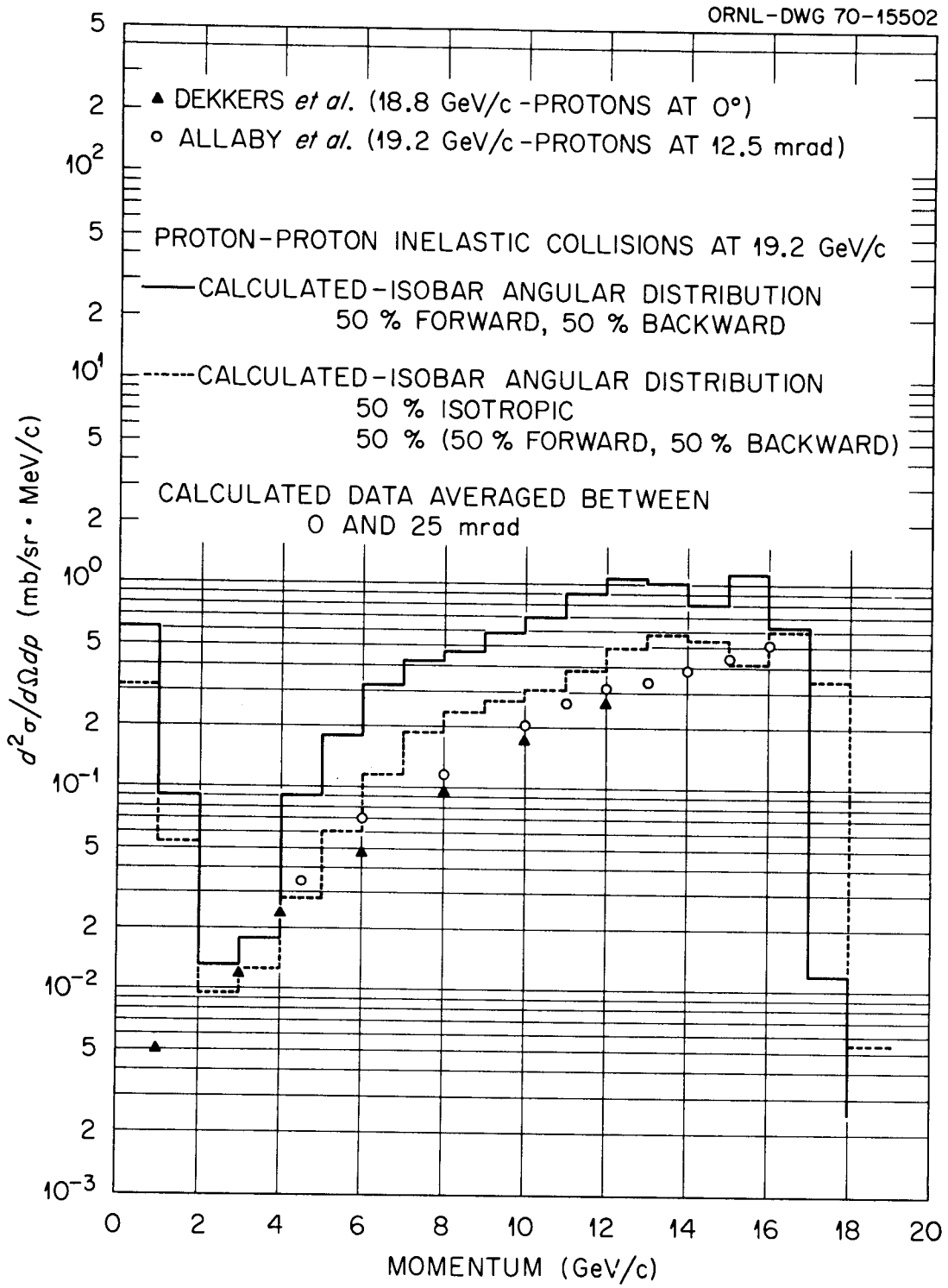

Fig. B1. Differential Proton Spectra at 12.5 mrad Resulting from Proton-Proton Inelastic Collisions at 19.2 GeV/c.

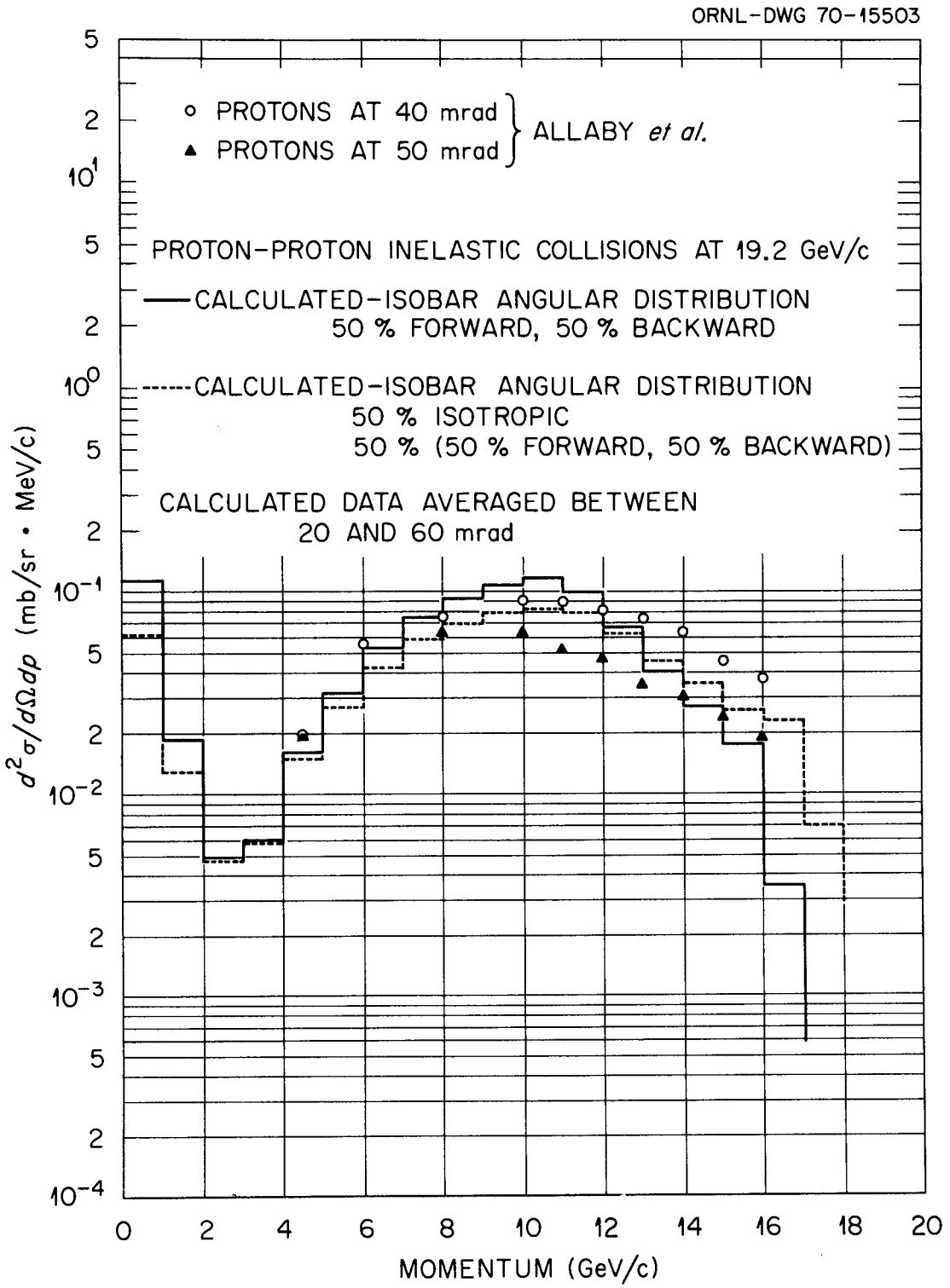

Fig. B2. Differential Proton Spectra at 40 mrad Resulting from Proton-Proton Inelastic Collisions at 19.2 GeV/c.

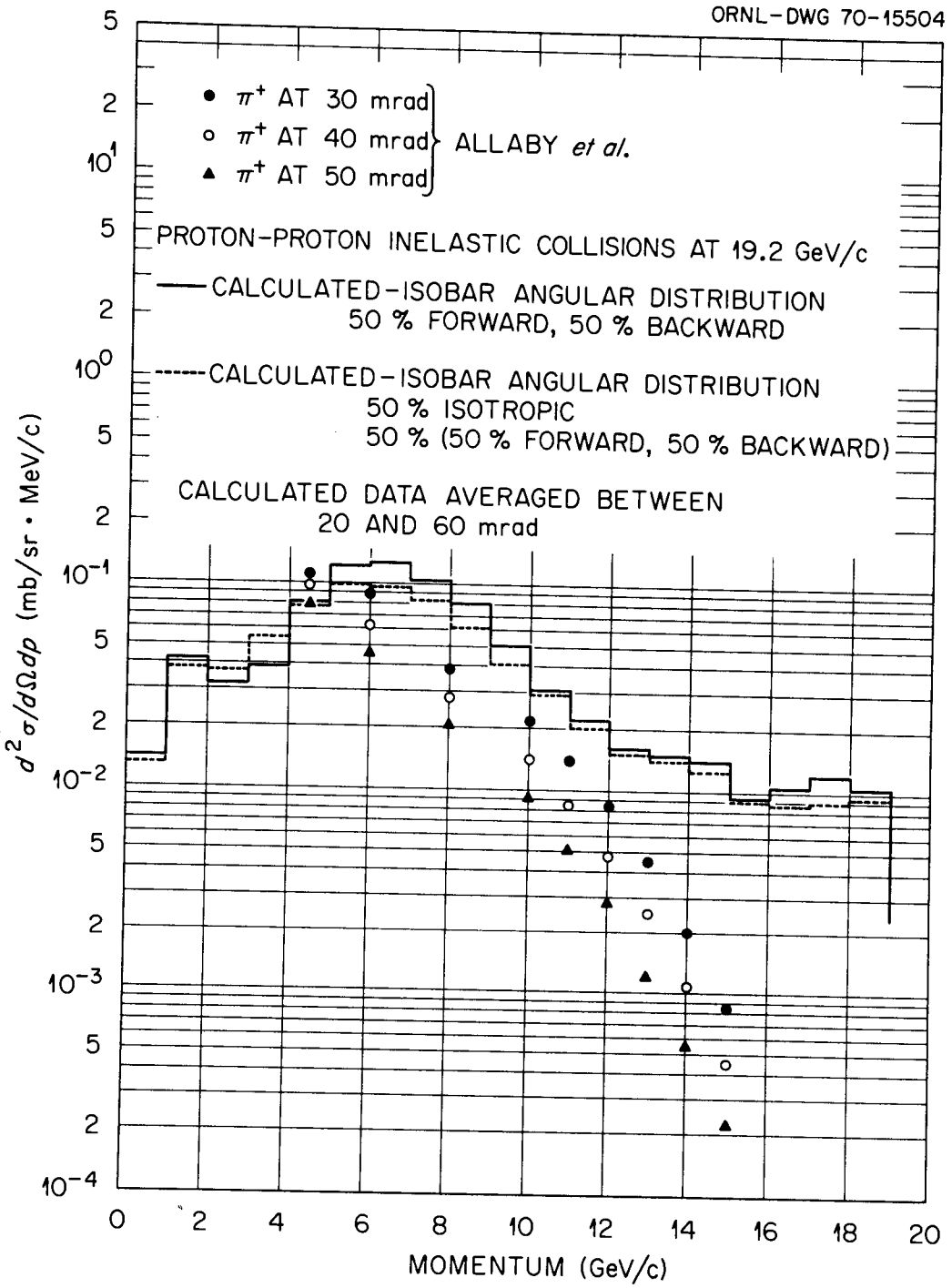

Fig. B3. Differential π^+ Spectra at 40 mrad Resulting from Proton-Proton Inelastic Collisions at 19.2 GeV/c.

REFERENCES

1) T. A. Gabriel, R. G. Alsmiller, Jr., and J. Barish, "Calculation of the Long-Lived Induced Activity in the Soil Around High-Energy Accelerator Target Areas - II," ORNL-4599, Oak Ridge National Laboratory (1970).

2) T. A. Gabriel, R. G. Alsmiller, Jr., and M. P. Guthrie, "An Extrapolation Method for Predicting Nucleon and Pion Differential Production Cross Sections from High-Energy (> 3 GeV) Nucleon-Nucleus Collisions," ORNL-4542, Oak Ridge National Laboratory (1970).

3) M. Awschalom et al., "Chemical Composition of Some Common Shielding Materials," TM-168(0160), National Accelerator Laboratory (1969).

4) T. W. Armstrong, R. G. Alsmiller, Jr., and K. C. Chandler, "Monte Carlo Calculations of High-Energy Nucleon-Meson Cascades and Applications to Galactic Cosmic-Ray Transport," to be presented at the National Symposium on Natural and Manmade Radiation in Space, Las Vegas, Nevada, March 1-5, 1971.

5) W. A. Coleman and T. W. Armstrong, "The Nucleon-Meson Transport Code NMTC," ORNL-4606, Oak Ridge National Laboratory (1970).

6) H. W. Bertini, M. P. Guthrie, and O. W. Hermann, "Instructions for the Operation of Codes Associated with MECC-3, a Preliminary Version of an Intranuclear-Cascade Calculation for Nuclear Reactions," ORNL-4564, Oak Ridge National Laboratory (in press).

7) Miriam P. Guthrie, "EVAP-4: Another Modification of a Code to Calculate Particle Evaporation from Excited Compound Nuclei," ORNL-TM-3119, Oak Ridge National Laboratory (1970).

8) See Appendix A and Appendix B.

9) R. M. Sternheimer and S. J. Lindenbaum, Phys. Rev. 109 (1958) 1723.

10) J. Ranft and T. Borak, "Improved Nucleon-Meson Cascade Calculations," FN-193, National Accelerator Laboratory (1969).

11) D. C. Irving et al., "05R, a General Purpose Monte Carlo Neutron Transport Code," ORNL-3622, Oak Ridge National Laboratory (1965).

12) T. A. Gabriel, Nucl. App. Tech. 9 (1970) 605.

13) H. W. Bertini, "Preliminary Data from Intranuclear-Cascade Calculations of 0.75-, 1-, and 2-GeV Protons on Oxygen, Aluminum, and Lead, and 1-GeV Neutrons on the Same Elements," ORNL-TM-1996, Oak Ridge National Laboratory (1967).

14) Hugo W. Bertini, Phys. Rev. 188 (1969) 1711; see also H. W. Bertini et al., "Intranuclear-Cascade Calculation of Secondary Nucleon Spectra from Nucleon-Nucleus Interactions in the Energy Range 340 to 2900 MeV and Comparison with Experiment," ORNL-TM-2361, Oak Ridge National Laboratory (1969).

15) H. W. Bertini et al., "Literature Survey of Radiochemical Cross-Section Data Below 425 MeV," ORNL-3884, Oak Ridge National Laboratory (1966).

16) H. W. Bertini, "Comparison of Calculated Radiochemical Cross Sections with Experimental Results for Incident Protons and π^- Mesons in the 50- to 400-MeV Region: Effect of Varying a Few Nuclear Parameters in the Calculations," ORNL-4105, Oak Ridge National Laboratory (1968).

17) W. Edward Alley et al., "Semiempirical Neutron-Induced Reaction Cross Sections," UCRL-50484, Lawrence Radiation Laboratory (1968).

18) S. G. Rudstam, Z. Naturforsch. 21a (1966) 1027, and Nucl. Phys. A126 (1969) 401.

[19] R. Bernas et al., Ann. Phys. 44 (1967) 426.

[20] F. Yiou et al., J. Geophys. Res., Space Phys., 74 (1969) 2447.

[21] E. L. Fireman and F. S. Rowland, Phys. Rev. 97 (1955) 780.

[22] G. Friedlander et al., Phys. Rev. 99 (1955) 263.

[23] M. Honda and D. Lal, Nucl. Phys. 51 (1964) 363.

[24] E. Baker et al., Phys. Rev. 112 (1958) 1319.

[25] H. W. Bertini, M. P. Guthrie, and A. H. Culkowski, "Phenomenologically Determined Isobar Angular Distributions for Nucleon-Nucleon and Pion-Nucleon Reactions Below 3 GeV," ORNL-TM-3132, Oak Ridge National Laboratory (1970).

[26] J. V. Allaby et al., "Particle Production in Proton-Proton Collisions at 19.2 GeV/c," in Proc. XIV International Conference on High-Energy Physics, Vienna, August 28-September 5, 1968.

[27] D. Dekkers et al., Phys. Rev. 137 (1965) B962.

Internal Distribution

1-3. L. S. Abbott
4. F. S. Alsmiller
5. R. G. Alsmiller, Jr.
6. T. W. Armstrong
7. H. W. Bertini
8. C. E. Clifford
9-28. T. A. Gabriel
29. M. P. Guthrie
30. W. E. Kinney
31. T. A. Love
32. F. C. Maienschein
33. R. W. Peelle
34. R. W. Roussin
35-44. R. T. Santoro
45. D. Sundberg
46. J. A. Turner
47. J. W. Wachter
48. H. A. Wright
49. W. Zobel
50. E. R. Cohen (consultant)
51. H. Feshbach (consultant)
52. H. Goldstein (consultant)
53. C. R. Mehl (consultant)
54. H. T. Motz (consultant)
55-56. Central Research Library
57. ORNL Y-12 Technical Library, Document Reference Section
58-59. Laboratory Records Department
60. Laboratory Records ORNL RC
61. ORNL Patent Office

External Distribution

62. P. B. Hemmig, Division of Reactor Development & Technology, U. S. Atomic Energy Commission, Washington, D. C.
63. W. H. Hannum, Division of Reactor Development & Technology, U. S. Atomic Energy Commission, Washington, D. C.
64. Kermit Laughon, AEC Site Representative.
65-161. Given AEC High-Energy Accelerator Shielding Distribution*.
162-176. Division of Technical Information (DTIE).
177. Laboratory and University Division (ORO).

*This distribution list is available upon request.